

An Efficient Ratio Detector for Ambient Backscatter Communication

Wenjing Liu, *Graduate Student Member, IEEE*, Shanpu Shen, *Member, IEEE*,
 Danny H. K. Tsang, *Fellow, IEEE*, Ranjan K. Mallik, *Fellow, IEEE*,
 Ross Murch, *Fellow, IEEE*

Abstract

Ambient backscatter communication (AmBC) leverages the existing ambient radio frequency (RF) environment to implement communication with battery-free devices. One critical challenge of AmBC systems is signal recovery because the transmitted information bits are embedded in the ambient RF signals and these are unknown and uncontrollable. To address this problem, most existing approaches use averaging-based energy detectors and consequently the data rate is low and there is an error floor. Here we propose a new detection strategy based on the ratio between signals received from a multiple-antenna Reader. The advantage of using the ratio is that ambient RF signals are removed directly from the embedded signals without averaging and hence it can increase data rates and avoid the error floor. Different from original ratio detectors that use the magnitude ratio of the signals between two Reader antennas, in our proposed approach, we utilize the complex ratio so that phase information is preserved and propose an accurate linear channel model approximation. This allows the application of existing linear detection techniques from which we can obtain a minimum distance detector and closed-form expressions for bit error rate (BER). In addition, averaging, coding and interleaving can also be included to further enhance the BER. The results are also general, allowing any number of Reader antennas to be utilized in the approach. Numerical results demonstrate that the proposed approach performs better than approaches based on energy detection and original ratio detectors.

Manuscript received; This work was supported by the Hong Kong Research Grants Council under General Research Fund grant 16207620. (*Corresponding author: Shanpu Shen.*)

W. Liu, S. Shen, R. Murch are with the Department of Electronic and Computer Engineering, The Hong Kong University of Science and Technology, Clear Water Bay, Kowloon, Hong Kong (e-mail: wliubj@connect.ust.hk; sshenaa@connect.ust.hk; eermurch@ust.hk).

D. H. K. Tsang is with The Hong Kong University of Science and Technology (Guangzhou), Nansha, Guangzhou, 511400, Guangdong, China, and the Department of Electronic and Computer Engineering, The Hong Kong University of Science and Technology, Clear Water Bay, Kowloon, Hong Kong (e-mail: eetsang@ust.hk).

Ranjan K. Mallik is with the Department of Electrical Engineering, Indian Institute of Technology - Delhi, Hauz Khas, New Delhi 110016, India (e-mail: rkmallik@ee.iitd.ernet.in).

Index Terms

Ambient backscatter communication, averaging, channel linearization, ratio detector, repetition code

I. INTRODUCTION

The Internet of things (IoT) has attracted significant attention in both academia and industrial circles [1]. Its function is to provide ubiquitous connectivity among a large number of small IoT computing devices (associated with people, homes, vehicles, and other factors) embedded in the environment and on and within people [2]. Powering the IoT devices is however challenging. Batteries have a limited lifetime and require significant maintenance costs to replace, while the use of solar energy requires the devices to be visible and in lighted regions.

One approach to meet the challenge of powering IoT devices is ambient backscatter communication (AmBC) which was first proposed by Liu *et. al* in 2013 [3]. In an AmBC system, a “Tag” harvests energy from ambient radio frequency (RF) signals to power its circuits [4], [5]. It transmits its data to a “Reader” by tuning its antenna impedance to reflect the received RF signals. Specifically, the Tag maps “0” and “1” bits to RF waveforms by adjusting the load impedance of the antenna between absorbing and reflecting states [6]. Different from conventional backscatter communication, e.g., Radio Frequency Identification (RFID), where a dedicated source of RF radiation is needed, AmBC enables battery-free Tags to communicate with other devices by harnessing ambient RF signals emitted from existing wireless systems (such as DTV [3], FM [7], [8], and Wi-Fi [9]-[12]). Thus, AmBC can operate without any dedicated RF source or extra frequency spectrum allocation, making it a promising approach for realizing a sustainable IoT ecosystem [2], [6]. In addition, the Reader does not require special duplexing circuitry (as in RFID Readers) so that existing devices, such as Wi-Fi, can potentially be modified to be Readers of AmBC signals.

In AmBC systems, the Reader receives two types of signals: the direct link signal emitted from the ambient RF source and the signal backscattered by the Tag. The backscattered signal is much weaker than the direct link signal due to the round-trip loss [13]. In addition, the ambient RF signal is unknown and uncontrollable. Therefore, the detection of AmBC signals transmitted by the Tag is challenging.

To tackle this challenge, averaging-based energy detection is a widely used method to recover the Tag data. The basic principle of the energy detector is to average the power of the received

signal and obtain its power level, which can be thresholded for detecting Tag symbols. In [3], the feasibility of communication between two battery-free devices utilizing ambient TV signals has been shown using averaging-based energy detection. The bit error rate (BER) performance of the energy detector with differential encoding and maximum-likelihood (ML) detector has also been investigated [14]-[16]. In [17], a joint energy detection scheme has been adopted where the differential coding characteristics have been exploited to avoid channel estimation and pilot symbols. The non-coherent energy detector has also been generalized to multiple-phase shift keying (MPSK) [18]. In [19], Manchester coding has been applied and an optimal non-coherent detector has been analyzed [20].

There are several disadvantages with the averaging-based energy detection approach. The first is that the averaging process significantly reduces the resulting bit rate. The averaging-based energy detection also has a severe error floor problem due to direct link interference [21]. That is, the BER converges to a nonzero floor with increase in the transmitted power from the ambient RF source [22]. Furthermore, energy detection generally suffers from performance loss since the averaging operation loses all the phase information [13].

Due to the limitations of averaging-based energy detection, enhancements to AmBC detection techniques have also been investigated. This includes implementing multiple antennas at the Reader to provide a straightforward method that can efficiently improve link quality and reliability and significantly increase the data rate. In [23], [24], blind energy detectors with multi-antenna Readers have been proposed. While the BER is lowered by increasing the number of antennas, the error floor caused by energy detectors still exists. Alternative approaches have also been considered, and this includes isolating the spectrum of the backscattered and ambient RF signals [25], [26], statistical clustering [22], and statistical covariances [27].

A very different approach to remove the ambient RF background signal from the transmitted bits has also been suggested in 2014, which is based on using the ratio of signals from separate antennas at the Reader [28]. It has been demonstrated that taking the ratio of two antenna branches at the Reader can cancel the ambient RF source, allowing increases in data rate [28]. Ratio detection is particularly suited to AmBC configurations that leverage systems such as Wi-Fi and where the AmBC Reader is integrated with the Wi-Fi station. This is because the ratio detector for AmBC can straightforwardly leverage the baseband outputs and synchronization from the Wi-Fi system to form the required ratio. The idea has been further investigated by finding an approximate detection threshold and the corresponding closed-form BER expression

has been derived [29]. As there is no error floor and data rates can be increased, the ratio detector approach has significant potential for further development.

In this paper, we take a new look at the AmBC Reader with ratio detection to overcome the drawbacks of conventional averaging-based energy detection. Our new contributions include:

1) Proposing a new ratio detector: Different from original ratio detectors [28], [29] that use magnitude information only, we propose using the direct ratio of the received signals so that the phase information is preserved. The probability density functions (PDFs) of the resulting statistic and optimal ML detector are also derived analytically.

2) Performing channel linearization: Using the proposed ratio allows us to develop an accurate channel linearization for the AmBC system. Based on the linear channel model, we simplify the ML detector to a minimum distance detector. The closed-form BER expression of the detector based on the proposed channel model is also presented.

3) Proposing averaging and coding techniques: Another advantage of having an accurate linear channel model for the AmBC system is that it provides a straightforward approach to averaging and coding. We show that the use of averaging, coding, and interleaving can further enhance the detection performance. Coding with and without interleaving is shown to be more effective than averaging as expected.

4) Generalizing to more than two antenna systems: The use of the ratio detector opens up the use of many types of ratios and their combinations when more than two antennas are utilized. We describe a straightforward ratio selection approach that efficiently lowers the BER for more than two antennas.

5) Numerical results: Comparisons between the proposed ratio detector, the conventional averaging-based energy detector, and the original ratio detector show the enhanced performance of our technique. For example, when the direct link signal-to-noise ratio (SNR) is 15 dB and $M = 1000$, the BER of the proposed detector is almost 100 times lower than averaging-based energy detection. The effectiveness of the proposed ratio selection scheme for more than two antennas is also shown.

In Section II, the system model of the proposed AmBC system with a multiple-antenna Reader is provided. In Section III, we introduce our proposed ratio detector. The resulting accurate linear channel approximation, minimum distance detector, and exact closed-form BER expressions of the detector are detailed. Section IV introduces averaging, coding, and interleaving while Section V generalizes the approach to arbitrary numbers of antennas. Section VI provides simulation

results and the conclusion is given in Section VII.

Notation: Bold lower and upper case letters denote vectors and matrices, respectively. A symbol not in bold font represents a scalar. x^* , $\Re\{x\}$, and $|x|$ refer to the conjugate, real part, and modulus, respectively, of a complex scalar x . \mathbf{x}^T refers to the transpose of a vector \mathbf{x} . $\text{diag}(\mathbf{x})$, returns a square diagonal matrix with the elements of vector \mathbf{x} on the main diagonal. \mathbb{R}^M denotes the space of M -dimensional real vectors. \mathbf{X}^T refers to the transpose of a matrix \mathbf{X} . $\mathcal{CN}(\mu, \sigma^2)$ refers to the circularly symmetric complex Gaussian distribution with mean μ and variance σ^2 . $f(\cdot)$ denotes the PDF of a random variable and $\Pr(\cdot)$ denotes the probability of an event.

II. SYSTEM MODEL

Consider an AmBC system consisting of an ambient RF source, a passive Tag equipped with a single antenna, and a Reader equipped with Q antennas as shown in Fig. 1. The ambient RF signal is denoted by $s(n)$ (with symbol period T_a), where $n = 1, 2, \dots$ is the symbol index of the ambient source. $s(n)$ is assumed random (and may come from different RF sources) and follows a circularly symmetric complex Gaussian distribution $\mathcal{CN}(0, P_s)$, where P_s denotes the average power of the ambient RF signal.

For the n th symbol period of the ambient source, the total signal received by the q th Reader antenna can be expressed as

$$z_q(n) = (A_{\text{SR}}h_q^{\text{SR}} + \alpha A_{\text{TR}}A_{\text{ST}}h_q^{\text{TR}}h^{\text{ST}}x) s(n) + w_q(n), \quad (1)$$

where A_{TR} and h_q^{TR} denote the large- and small-scale channel fading between the Tag antenna and the q th Reader antenna, A_{ST} and h^{ST} denote the large- and small-scale channel fading between the ambient RF source and the Tag antenna, A_{SR} and h_q^{SR} , respectively, denote the large- and small-scale channel fading between the ambient RF source and the q th Reader antenna. The symbol transmitted by the Tag antenna is denoted as x , and $w_q(n)$ is the additive white Gaussian noise (AWGN) at the q th Reader antenna. Besides, we assume block-fading, where the channel coherence time exceeds the transmission duration of a block. However, the channel will still vary from one block to another because multi-path components are varying over time [30].

We assume h_q^{SR} , $h_q^{\text{TR}} \forall q$, and h^{ST} are independent and identically distributed (i.i.d.), quasi-static, and frequency flat. We also assume $A_{\text{SR}} \approx A_{\text{ST}}$ since the Tag and the Reader are close

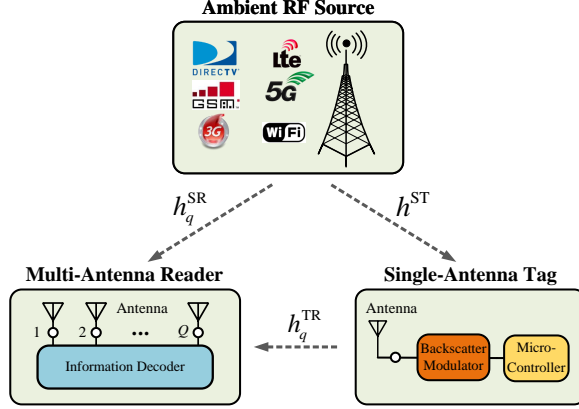


Fig. 1. System model of an AmBC system with a single-antenna Tag and a multiple-antenna Reader.

to each other. Therefore, we can normalize (1) by A_{SR} to equivalently rewrite (1) as

$$\bar{z}_q(n) = (h_q^{\text{SR}} + h_q^{\text{TR}} g x) s(n) + \bar{w}_q(n), \quad (2)$$

where we define $\bar{z}_q(n) = z_q(n)/A_{\text{SR}}$, $g = \alpha A_{\text{TR}} h^{\text{ST}}$ and $\bar{w}_q(n) = w_q(n)/A_{\text{SR}}$. We assume $\bar{w}_q(n) \sim \mathcal{CN}(0, N_w)$ where N_w denotes the normalized noise power.

Leveraging (2), we can define the direct link SNR γ_d as

$$\gamma_d \triangleq \frac{P_s}{N_w}, \quad (3)$$

which is the ratio of ambient RF signal power and normalized noise power at the Reader. This is referred to as SNR in the remainder of the paper. We also define a relative SNR $\Delta\gamma$ as

$$\Delta\gamma \triangleq \frac{1}{\alpha^2 A_{\text{TR}}^2}, \quad (4)$$

which is the ratio of the signal power from the direct link and the backscatter link. The relative SNR $\Delta\gamma$ is usually greater than 30 dB and therefore special techniques need to be utilized for AmBC signal detection [31].

The most common detection approach in AmBC is averaging-based energy detection but it suffers from performance issues as discussed earlier. As an alternative approach, it is possible to consider the ratio between two antenna branches (say $q = 1$ and 2) as it can effectively cancel or divide out the unknown ambient RF source signal $s(n)$. Not only can this overcome the error floor of conventional averaging-based energy detection, it can also increase the data rate. The

originally proposed ratio detector uses the magnitude ratio of the received signals at two antenna branches [28], [29]. It is shown that the ratio detector avoids the error floor phenomenon faced by averaging-based energy detector [29], with the data rate and communication range having been greatly improved [28]. However, taking the magnitude ratio loses potentially useful phase information, and also makes the channel model nonlinear. In [28], it is pointed out that the use of magnitudes allows the use of non-coherent receivers. However, with AmBC Readers being integrated in systems such as Wi-Fi, signals received by different antenna branches will be phase coherent due to the use of a single local oscillator. This allows the consideration of complex signal ratios. An advantage of using complex ratios is that an accurate linear channel model can be developed for AmBC as shown next.

III. PROPOSED RATIO DETECTOR

We firstly analyze the system performance of the ratio detector with $Q = 2$ antenna branches to highlight its functionality. Later in Section V we provide a straightforward generalization for $Q > 2$ antennas.

We denote the signal ratio between the two antenna ($q = 1, 2$) branches as

$$\lambda(n) = \frac{\bar{z}_1(n)}{\bar{z}_2(n)} = \frac{(h_1^{\text{SR}} + h_1^{\text{TR}}gx) s(n) + \bar{w}_1(n)}{(h_2^{\text{SR}} + h_2^{\text{TR}}gx) s(n) + \bar{w}_2(n)}. \quad (5)$$

This is different from the originally proposed ratio detector as we have removed the magnitude or modulus operation. The advantage of using this ratio is that it allows us to develop an accurate linear channel model for the AmBC system. Subsequently, the use of linear detectors, averaging, and coding can be utilized.

One issue in forming the ratio (5) is retaining its phase. However, proposed AmBC Readers are likely to be integrated with existing wireless systems such as Wi-Fi. In these circumstances, the system will be coherent and phase coherence will exist between antenna branches. Therefore, extracting the I and Q signals for each antenna branch and taking the ratio will not likely require additional information. This is a significant advantage of using this ratio.

A. PDF and ML detection

In this paper, for simplicity we focus on using BPSK modulation for the transmit signal x , that is, $x = \pm 1$. Other common modulation techniques such as ASK, PSK and QAM, can also be applied in the proposed ratio detector. Defining $\mu_q = h_q^{\text{SR}} + h_q^{\text{TR}}gx$, $q = 1, 2$, as the composite

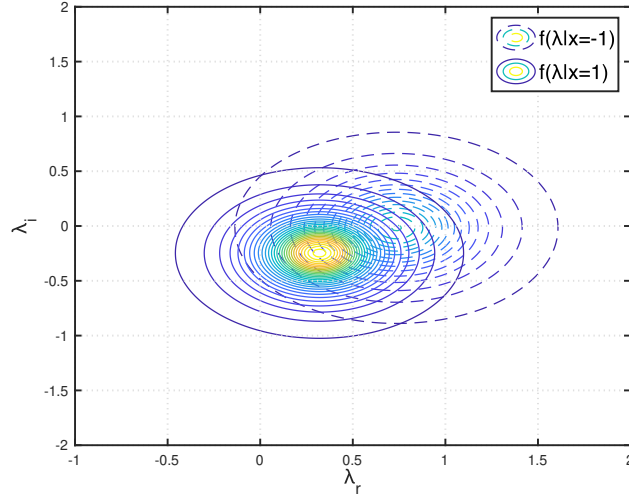


Fig. 2. Example PDFs of two backscatter states for the proposed ratio detector when $\gamma_d = 10$ dB.

channel between the Reader and Tag when $x = \pm 1$ allows us to write $\mu_q s(n) + \bar{w}_q(n) \sim \mathcal{CN}(0, \sigma_q^2)$ where $\sigma_q^2 = |\mu_q|^2 P_s + N_w$, $q = 1, 2$.

Since $\lambda(n)$ is a ratio of two complex Gaussian distributed random variables, according to [32], [33], its PDF is given by

$$f(\lambda) = \frac{1 - |\rho|^2}{\pi \sigma_1^2 \sigma_2^2} \left(\frac{|\lambda|^2}{\sigma_1^2} + \frac{1}{\sigma_2^2} - 2 \frac{\rho_r \lambda_r - \rho_i \lambda_i}{\sigma_1 \sigma_2} \right)^{-2}, \quad (6)$$

where λ_r and λ_i represent the real and imaginary parts of λ , respectively; ρ_r and ρ_i represent the real and imaginary parts, respectively, of ρ , which is the complex correlation coefficients between $\bar{z}_1(n)$ and $\bar{z}_2(n)$ and is written as

$$\rho = \frac{\mu_1^* \mu_2 P_s}{\sigma_1 \sigma_2}. \quad (7)$$

The resulting PDFs for an example channel realization with $f(\lambda|x=-1)$ and $f(\lambda|x=1)$ are shown in Fig. 2 when the direct link SNR is 10 dB.

In ML detection, the goal is to design an optimal detector that can minimize the error probability, or equivalently, maximize the correct decision probability

$$\hat{x} = \arg \max_{x \in \{-1, 1\}} \Pr(x|\lambda). \quad (8)$$

Since the transmit messages $x = -1$ and $x = 1$ are equiprobable, according to Baye's theorem,

the ML criterion is written as

$$\hat{x} = \begin{cases} -1, & \text{if } f(\lambda | x = -1) \geq f(\lambda | x = 1) \\ 1, & \text{if } f(\lambda | x = -1) < f(\lambda | x = 1) \end{cases}. \quad (9)$$

That is, we substitute the obtained λ in (6), and then determine x by comparing the size relationship of two posterior density functions. Channel state information (CSI) is also required for evaluating (9). Several channel estimation methods have been demonstrated previously that can provide accurate CSI [34]-[39] and in the remainder of this paper we assume the Reader has perfect CSI.

The optimal ML detector is computationally intricate since it needs to compute intricate PDFs and it is not linear. It can also be observed that determining a signal threshold for detection is difficult. The intricacy of ML detection can be completely avoided by utilizing a different approach. It is shown next that the channel model (5) can be accurately approximated by a linear channel model under the conditions of AmBC. This allows us to devise a straightforward minimum distance detector. In addition it opens up the use of all of the linear detection tools available such as averaging, coding, and selection diversity.

B. Linearization of Proposed Ratio Detector

Utilizing the complex ratio (5), we develop an accurate channel linearization for AmBC. We rewrite the ratio $\bar{z}_1(n)/\bar{z}_2(n)$ as

$$\frac{\bar{z}_1(n)}{\bar{z}_2(n)} = \frac{h_1^{\text{SR}} \left(1 + \frac{h_1^{\text{TR}} g x}{h_1^{\text{SR}}} + \frac{\bar{w}_1(n)}{h_1^{\text{SR}} s(n)} \right)}{h_2^{\text{SR}} \left(1 + \frac{h_2^{\text{TR}} g x}{h_2^{\text{SR}}} + \frac{\bar{w}_2(n)}{h_2^{\text{SR}} s(n)} \right)}. \quad (10)$$

Taking logarithms we have

$$\log \left(\frac{\bar{z}_1(n)}{\bar{z}_2(n)} \right) = \log \left(\frac{h_1^{\text{SR}}}{h_2^{\text{SR}}} \right) + \log \left(1 + \frac{h_1^{\text{TR}} g x}{h_1^{\text{SR}}} + \frac{\bar{w}_1(n)}{h_1^{\text{SR}} s(n)} \right) - \log \left(1 + \frac{h_2^{\text{TR}} g x}{h_2^{\text{SR}}} + \frac{\bar{w}_2(n)}{h_2^{\text{SR}} s(n)} \right). \quad (11)$$

Under typical AmBC conditions, the direct link (ambient RF source to Reader) has a significantly higher channel gain than the indirect link (ambient RF source to Tag and then backscattered to Reader). This corresponds to the fact that the relative SNR $\Delta\gamma$ in practical AmBC systems is usually higher than 30 dB [31]. Therefore, with $q = 1, 2$, the signals very frequently satisfy

the conditions

$$|h_q^{\text{TR}}gx| \ll |h_q^{\text{SR}}|; \quad (12)$$

$$|\bar{w}_q(n)| \ll |s(n)h_q^{\text{SR}}|. \quad (13)$$

Under these conditions it can be readily seen that

$$\left| \frac{h_q^{\text{TR}}gx}{h_q^{\text{SR}}} + \frac{\bar{w}_q(n)}{h_q^{\text{SR}}s(n)} \right| \rightarrow 0. \quad (14)$$

Using the limit that $\log(1+x) \rightarrow x$ when $x \rightarrow 0$ and the property (14), we have

$$\log \left(1 + \frac{h_q^{\text{TR}}gx}{h_q^{\text{SR}}} + \frac{\bar{w}_q(n)}{h_q^{\text{SR}}s(n)} \right) \rightarrow \frac{h_q^{\text{TR}}gx}{h_q^{\text{SR}}} + \frac{\bar{w}_q(n)}{h_q^{\text{SR}}s(n)}. \quad (15)$$

Thus, (11) can be expressed as

$$\log \left(\frac{\bar{z}_1(n)}{\bar{z}_2(n)} \right) = \log \left(\frac{h_1^{\text{SR}}}{h_2^{\text{SR}}} \right) + \left(\frac{h_1^{\text{TR}}}{h_1^{\text{SR}}} - \frac{h_2^{\text{TR}}}{h_2^{\text{SR}}} \right) gx + \left(\frac{\bar{w}_1(n)}{h_1^{\text{SR}}} - \frac{\bar{w}_2(n)}{h_2^{\text{SR}}} \right) \frac{1}{s(n)}. \quad (16)$$

The constant bias term $\log(h_1^{\text{SR}}/h_2^{\text{SR}})$ in (16) can be estimated and removed. Let us define $\hat{y} \triangleq \log(\bar{z}_1(n)/\bar{z}_2(n)) - \log(h_1^{\text{SR}}/h_2^{\text{SR}})$; according to (16), we can obtain

$$\hat{y} = hx + \tilde{w}, \quad (17)$$

where h is defined as

$$h \triangleq \left(\frac{h_1^{\text{TR}}}{h_1^{\text{SR}}} - \frac{h_2^{\text{TR}}}{h_2^{\text{SR}}} \right) g, \quad (18)$$

and \tilde{w} is defined as

$$\tilde{w} \triangleq \left(\frac{\bar{w}_1(n)}{h_1^{\text{SR}}} - \frac{\bar{w}_2(n)}{h_2^{\text{SR}}} \right) \frac{1}{s(n)}. \quad (19)$$

Note that $(\bar{w}_1(n)/h_1^{\text{SR}} - \bar{w}_2(n)/h_2^{\text{SR}})$ still follows a complex Gaussian distribution, so \tilde{w} is a ratio of two complex Gaussian variables. According to [32], the PDF of \tilde{w} can be obtained as

$$f(\tilde{w}) = \frac{N_w}{\pi P_s} \left(\frac{1}{|h_1^{\text{SR}}|^2} + \frac{1}{|h_2^{\text{SR}}|^2} \right) \left(|\tilde{w}|^2 + \left(\frac{1}{|h_1^{\text{SR}}|^2} + \frac{1}{|h_2^{\text{SR}}|^2} \right) \frac{N_w}{P_s} \right)^{-2}. \quad (20)$$

A further detail is that herein we only take the principal value of each logarithm. As a result, the phase of $\log(\bar{z}_1(n)/\bar{z}_2(n))$ is restricted to $(-\pi, \pi]$ while the right-hand side of (11) has a phase in $(-3\pi, 3\pi]$. Therefore, it is possible that the phase of the right-hand side of (11) has $\pm 2\pi$

shift with $\log(\bar{z}_1(n)/\bar{z}_2(n))$. Consequently, (17) does not always hold. Thus, we cannot utilize (17) directly to detect the Tag data since the phase shift will decrease the detection performance. In order to reduce its influence, we propose a phase compensation method.

Recall that the direct link has a significantly higher channel gain than the indirect link. Thus $\log(h_1^{\text{SR}}/h_2^{\text{SR}})$ is dominant in $\log(\bar{z}_1(n)/\bar{z}_2(n))$ and we can compare the phase of them to reveal if there is a 2π phase shift. After removing the bias $\log(h_1^{\text{SR}}/h_2^{\text{SR}})$, the extra phase $\Delta\phi$ that needs to be compensated on \hat{y} is

$$\Delta\phi = \begin{cases} 2\pi & , \text{if } \phi\left(\log\left(\frac{\bar{z}_1(n)}{\bar{z}_2(n)}\right)\right) - \phi\left(\log\left(\frac{h_1^{\text{SR}}}{h_2^{\text{SR}}}\right)\right) < -\pi \\ -2\pi & , \text{if } \phi\left(\log\left(\frac{\bar{z}_1(n)}{\bar{z}_2(n)}\right)\right) - \phi\left(\log\left(\frac{h_1^{\text{SR}}}{h_2^{\text{SR}}}\right)\right) > \pi \\ 0 & , \text{otherwise} \end{cases}, \quad (21)$$

where $\phi(\log(\bar{z}_1(n)/\bar{z}_2(n)))$ and $\phi(\log(h_1^{\text{SR}}/h_2^{\text{SR}}))$ represent the phase of $\log(\bar{z}_1(n)/\bar{z}_2(n))$ and $\log(h_1^{\text{SR}}/h_2^{\text{SR}})$, respectively.

The modified (17) is then written as

$$y = \hat{y} + j\Delta\phi = hx + \tilde{w}, \quad (22)$$

which is the finalized linear channel model for the proposed ratio detector and $j = \sqrt{-1}$. The effectiveness of phase compensation will be shown in Section VI.

In summary, by performing the logarithm approximation (16), removing bias, and compensating phase shift (21), we can approximate the ratio channel model in AmBC (5) as a linear channel model (22). This channel model approximation is accurate for most practical configurations in AmBC as shown later in Section VI.

C. Minimum Distance Detector

The computational complexity of the optimal ML detector (9) can be reduced by leveraging the linearized AmBC channel model to simplify the detection process.

For simplicity, we further define τ as

$$\tau \triangleq \left(\frac{1}{|h_1^{\text{SR}}|^2} + \frac{1}{|h_2^{\text{SR}}|^2} \right) \frac{N_w}{\pi P_s}. \quad (23)$$

The ML detector is then given by

$$\begin{aligned}\hat{x} &= \arg \max_{x \in \{-1,1\}} f(y|x) \\ &= \arg \max_{x \in \{-1,1\}} \tau (|y - hx|^2 + \pi\tau)^{-2}.\end{aligned}\quad (24)$$

It can be readily checked that the function to be maximized in (24) is monotonically decreasing with $|y - hx|^2$. Thus (24) can be simplified as

$$\hat{x} = \arg \min_{x \in \{-1,1\}} |y - hx|^2, \quad (25)$$

where h is given by (18). It implies that the ML detector (9) can be reduced to a minimum distance detector.

To conclude, based on the proposed linearized AmBC channel model (22), we can apply linear detection to detect x and avoid computing the complicated PDF functions (6). Therefore, the computational complexity for detection is greatly reduced without a reduction in performance as shown in Section VI.

D. BER Analysis

Utilizing the linear AmBC channel model, we can provide a BER analysis for the proposed minimum distance detector.

Suppose we transmit x in a single transmission. According to (25), the error event is the distance between the received signal y and hx is larger than $-hx$. Equivalently,

$$|y - hx|^2 > |y + hx|^2; \quad (26)$$

in other words,

$$\Re \{hx\tilde{w}\} < -|h|^2. \quad (27)$$

Let $\varphi = hx\tilde{w}$, and φ_r and φ_i represent the real and imaginary parts, respectively, of φ . It can be readily seen that φ is also a ratio of complex Gaussian variables. Thus, the error probability can be expressed as

$$P_b = \int_{-\infty}^{-|h|^2} \int_{-\infty}^{\infty} f(\varphi) d\varphi_i d\varphi_r, \quad (28)$$

where

$$f(\varphi) = \tau |h|^2 (\varphi_r^2 + \varphi_i^2 + \pi\tau |h|^2)^{-2}. \quad (29)$$

To obtain the closed-form expression of P_b , the indefinite integral of $f(\varphi)$ should be found. In [32], it is pointed out that the integral of the PDF (29) can be expressed in closed-form as

$$\iint f(\varphi) d\varphi_i d\varphi_r = \zeta(\varphi_r, \varphi_i) + \zeta(\varphi_i, \varphi_r) = G(\varphi_r, \varphi_i), \quad (30)$$

where

$$\zeta(\varphi_r, \varphi_i) = \frac{\gamma(z_i)}{2\pi} \cdot \arctan\left(\frac{\varphi_r}{\sqrt{\pi\tau |h|^2 + \varphi_i^2}}\right), \quad (31)$$

and

$$\gamma(z_i) = \frac{\varphi_i}{\sqrt{\pi\tau |h|^2 + \varphi_i^2}}. \quad (32)$$

The BER P_b is therefore expressed as

$$P_b = G(-|h|^2, \infty) + G(-\infty, -\infty) - G(\infty, -\infty) - G(-|h|^2, -\infty), \quad (33)$$

where the function G is given by (30).

Substituting (30) in (33), we obtain a *closed-form BER expression* as

$$P_b = \frac{1}{2} - \frac{1}{2\sqrt{\frac{\pi\tau}{|h|^2} + 1}}. \quad (34)$$

It can be seen that, by using the approximate linear channel model, an exact closed-form BER expression can be found, which again shows the benefit of channel linearization. Since we leverage the phase information, it can be expected that (34) has lower BER than the original ratio detector. The BERs of the proposed ratio detector and the original ratio detector are numerically compared in Section VI.

IV. AVERAGING AND CODING

While the previous results can be utilized directly to achieve AmBC with high data rates, the strong interference from the direct link limits performance. To overcome this challenge, three approaches are proposed: 1) symbol averaging, 2) coding with hard and soft detection, and 3) coding and interleaving. The formulations and advantages of each of these are detailed next.

A. Averaging

Due to the development of the linear channel model (22), it is possible to implement straightforward averaging to enhance the performance. While not an optimum approach, it is computationally straightforward.

Expanding the duration of the Tag data is equivalent to transmit bit repetition. The expansion duration, averaging period, or repetition length is taken as M symbols. It is assumed the channel coherence time is K symbols. To leverage the coherence of the channel, M is less than K . For formulation convenience, however, we take $M = K$, without loss of generality.

We assume that an arbitrary incoming bit stream at the tag is written as x_1, x_2, \dots . Since the bits are independent, we consider a single bit x_k . The duration of bit x_k is expanded M times to form a transmit vector $\mathbf{x}_k = [x_k; x_k; \dots; x_k]$ of dimension M . At the Reader side, for k th received expanded or repeated signal block, we have

$$\mathbf{y}_k = h_k \mathbf{x}_k + \tilde{\mathbf{w}}_k, \quad (35)$$

where $\mathbf{y}_k = [y_{1,k}; y_{2,k}; \dots; y_{m,K}; \dots; y_{M,k}]$ represents the k th received block and $y_{m,k}$ represents the m th received signal of the k th block, h_k denotes the channel realization of the k th block, and $\tilde{\mathbf{w}}_k = [\tilde{w}_{1,k}; \tilde{w}_{2,k}; \dots; \tilde{w}_{m,K}; \dots; \tilde{w}_{M,K}]$ is the noise vector, where $\tilde{w}_{m,k}$ represents the noise in $y_{m,k}$.

Due to the linearity and channel coherence, we can average over y_k to decode x_k to obtain

$$\hat{x}_k = \arg \max_{x_k \in \{-1,1\}} f(\bar{y}_k | x_k), \quad (36)$$

where \bar{y}_k is the averaged received signal

$$\bar{y}_k = \frac{\sum_{m=1}^M y_{m,k}}{M}. \quad (37)$$

Since the averaged signal \bar{y}_k has the same distribution as $y_{m,k}, \forall m$, (36) can be written as

$$\hat{x}_k = \arg \min_{x_k \in \{-1,1\}} |\bar{y}_k - h_k x_k|^2. \quad (38)$$

Since the noise is independent for each repeated bit, we can expect the noise to be averaged while the desired signal adds coherently. Therefore a doubling of M will result in an approximately 3 dB increase in the SNR (not exactly 3 dB because of the channel linearization

approximation) and the performance will improve.

B. Coding without Interleaving

Coding can be utilized as a more effective form of averaging. However, to achieve the necessary gain in performance required, we need to select very low coding rates such as 1/500 or higher. Therefore, conventional codes as used in terrestrial communications cannot be utilized. For this reason, we utilize the conventional repetition code with very low coding rates. Hard and soft detection are considered.

For the repetition code, the encoding and transmission processes are the same as the averaging method. For the hard decision method, recall that x_k is related to M received signals, and

$$y_{m,k} = h_k x_k + \tilde{w}_{m,k}, \quad m = 1, \dots, M. \quad (39)$$

For each signal, we can use the minimum distance detector (25) to decode it. Thus, for bit x_k , there will be M decisions and we take the majority as the final decision, which is

$$\hat{x}_k = \begin{cases} 1 & \text{if number of 1's} \geq -1's \\ -1 & \text{if number of 1's} < -1's \end{cases}. \quad (40)$$

For soft decision detection, our detection rule is

$$\begin{aligned} \hat{x}_k &= \arg \max_{x_k \in \{-1, 1\}} f(\mathbf{y}_k | x_k) \\ &= \arg \max_{x_k \in \{-1, 1\}} \prod_{m=1}^M f(y_{m,k} | x_k) \\ &= \arg \min_{x_k \in \{-1, 1\}} \sum_{m=1}^M \log(|y_{m,k} - h_k x_k|^2 + \pi \tau_k), \end{aligned} \quad (41)$$

where $\tau_k = \left(1 / |h_{1,k}^{\text{SR}}|^2 + 1 / |h_{2,k}^{\text{SR}}|^2\right) N_w / (\pi P_s)$, and $h_{q,k}^{\text{SR}}$ represents the small-scale fading between the ambient source and the q th Reader antenna of the k th block.

Although the repetition code has the same operation as averaging at the Tag side, since hard and soft decision detection methods consider more information about the received signals, e.g., PDF for soft decision, it can be expected that this coding scheme will outperform averaging. The comparison is shown in Section VI.

C. Coding with Interleaving

To further combat deep fading, interleaving is combined with the repetition code. During interleaving, the transmitted data is arranged over multiple code blocks by the interleaver before backscattering. Due to this, the block experiencing deep fading is spread out among multiple blocks. When the Reader rearranges the blocks, the errors appear as independent random errors or burst errors with short lengths, which are much easier to detect.

Extending the formulations of Section IV.A and Section IV.B, we form a block \mathbf{X} as

$$\mathbf{X} = [\mathbf{x}_1, \mathbf{x}_2, \dots, \mathbf{x}_k, \dots, \mathbf{x}_K]. \quad (42)$$

Applying interleaving, \mathbf{X} is rearranged using a transpose operation as

$$\mathbf{V} = \mathbf{X}^T = [\mathbf{v}_1, \mathbf{v}_2, \dots, \mathbf{v}_m, \dots, \mathbf{v}_M], \quad (43)$$

where $\mathbf{v}_m = [x_1; x_2; \dots; x_k, \dots, x_K]$ is a K dimensional vector representing the transmitting bit stream during the m th block time. Now each repetition codeword is rearranged into M blocks.

At the Reader side, after channel linearization, the received signal matrix during M coherent time slots is given by

$$\mathbf{Y} = \mathbf{V} \text{diag}(\mathbf{h}) + \tilde{\mathbf{W}} = [\mathbf{y}_1, \mathbf{y}_2, \dots, \mathbf{y}_m, \dots, \mathbf{y}_M], \quad (44)$$

where $\mathbf{y}_m = h_m \mathbf{v}_m + \tilde{\mathbf{w}}_m$ denotes the signal received in the m th block. $\mathbf{h} = [h_1; h_2; \dots, h_m; \dots, h_M]$ denotes the channel vector of M blocks where h_m denotes the m th realization of channel h . $\tilde{\mathbf{W}} = [\tilde{\mathbf{w}}_1, \tilde{\mathbf{w}}_2, \dots, \tilde{\mathbf{w}}_m, \dots, \tilde{\mathbf{w}}_M]$ is the noise matrix where $\tilde{\mathbf{w}}_m = [\tilde{w}_{1,m}; \tilde{w}_{2,m}; \dots; \tilde{w}_{k,m}; \dots; \tilde{w}_{K,m}]$ is the noise vector with $\tilde{w}_{k,m}$ representing the noise of the k th received signal in the m th block. It can be seen that x_k experiences M channels during interleaving, which offers channel diversity to help detect the signal.

A deinterleaver is used to recover each repetition code. After rearranging the received matrix \mathbf{Y} , we have

$$\mathbf{R} = \mathbf{Y}^T = [\mathbf{r}_1, \mathbf{r}_2, \dots, \mathbf{r}_k, \dots, \mathbf{r}_K], \quad (45)$$

where

$$\mathbf{r}_k = [r_{k,1}; r_{k,2}; \dots, r_{k,m}; \dots, r_{k,M}] = \mathbf{h} x_k + \mathbf{u}_k, \quad (46)$$

with $\mathbf{u}_k = [\tilde{w}_{k,1}; \tilde{w}_{k,2}; \dots; \tilde{w}_{k,m}; \dots; \tilde{w}_{k,M}]$ representing the noise vector.

Algorithm 1 Averaging, Coding and Interleaving

Initialize: K is the channel coherent time and M is the codeword length of the repetition code.

$K = M$. x_1, x_2, \dots, x_K are modulated using BPSK.

1: Encoding: $\mathbf{X} = [\mathbf{x}_1, \mathbf{x}_2, \dots, \mathbf{x}_k, \dots, \mathbf{x}_K]$, $\mathbf{x}_k = [x_k; x_k; \dots; x_k] \in \mathbb{R}^M$

2: **if without interleaving**

3: **for** $k = 1 : K$

4: Obtain \mathbf{y}_k by (35)

5: **if averaging**

6: Obtain \bar{y}_k by (37)

7: Obtain \hat{x}_k by (38)

8: **end**

9: **if hard decision**

10: Obtain \hat{x}_k by (40)

11: **end**

12: **if soft decision**

13: Obtain \hat{x}_k by (41)

14: **end**

15: **end**

16: **end**

17: **if with interleaving**

18: Obtain \mathbf{V} , \mathbf{Y} , and \mathbf{R} by (43)–(45)

19: **for** $k = 1 : K$

20: Repeat step 9 – 14

21: **end**

22: **end**

Return $\hat{\mathbf{x}} = [\hat{x}_1; \hat{x}_2; \dots; \hat{x}_k, \dots, \hat{x}_K]$

Since each repetition code is independent, we can use \mathbf{r}_1 to \mathbf{r}_K to decode x_1 to x_K . Correspondingly hard and soft decision detection can then be applied similarly to that without interleaving.

Compared with Section IV.A and Section IV.B, it can be seen that since interleaving is utilized, the encoding and detection complexity is increased for this scheme. However, the channel diversity can significantly lower BER, which will be verified in Section VI.

The overall algorithm for the transmission and decoding process for the three proposed schemes is summarized in Algorithm 1. It should be noted that the channel vector \mathbf{h} is obtained based on the proposed linear channel model, without which the soft decision and hard decision processes will be difficult to implement.

V. OPTIMUM RATIO SELECTION SCHEME

In this section, we generalize the ratio detector to Readers with $Q > 2$ antennas. With $Q > 2$ Reader antennas, there are a variety of ratios that can be considered, as well as many methods to utilize them. For example, the ratio need not be the straightforward ratio of a pair. The resulting ratios can also be combined in various ways including some form of maximal ratio combining. The full investigation of detectors for dealing with $Q > 2$ receive antennas can therefore be seen to be a significant undertaking.

To demonstrate the potential of our proposed ratio detector, and averaging, coding, and interleaving techniques with $Q > 2$, we restrict our approach to the most straightforward system and leave the investigation of the complete generalization to future work. As such we restrict the ratios to be between pairs of antenna branches and then propose an optimal ratio selection scheme to leverage selection diversity. Even this straightforward approach provides significant improvements in performance as shown later in the simulation results section.

Our goal is to select the optimal ratio to minimize the BER (34). Accordingly, the optimization problem can be formulated as

$$\mathbf{P1} : \min_{i,j} \frac{1}{2} - \frac{1}{2\sqrt{\frac{\pi\tau_{i,j}}{|h_{i,j}|^2} + 1}} \quad (47)$$

$$\text{s.t. } i, j \in \{1, 2, \dots, Q\}, i \neq j \quad (48)$$

where $\tau_{i,j}$ and $h_{i,j}$ represent the value of τ and h calculated with the i th and j th antenna pairs, $i, j \in \{1, 2, \dots, Q\}, i \neq j$.

To solve this problem, we first observe that P_b monotonically increases with $\eta_{i,j}$, which is given by

$$\eta_{i,j} = \frac{\pi P_s |g|^2}{N_w} \cdot \frac{\tau_{i,j}}{|h_{i,j}|^2} = \frac{\frac{1}{|h_i^{\text{SR}}|^2} + \frac{1}{|h_j^{\text{SR}}|^2}}{\left| \frac{h_i^{\text{TR}}}{h_i^{\text{SR}}} - \frac{h_j^{\text{TR}}}{h_j^{\text{SR}}} \right|^2}, \quad (49)$$

where subscript i, j denotes a parameter related to the i, j th antenna pair. Since η is only related to the channel parameters of the two branches in the ratio, by selecting a ratio with the minimum value of η among all the ratios, a lower BER can be obtained.

With Q Reader antennas, $Q(Q-1)$ ratio pairs can be formed. It should be noted that for each ratio pair, swapping the numerator and denominator does not affect the value of η . Thus we further restrict to $i < j$, and only $Q(Q-1)/2$ ratios need to be searched.

Algorithm 2 Optimal Ratio Selection Scheme

Initialize: Channel parameters $h_q^{\text{SR}}, h_q^{\text{ST}}, q \in \{1, 2, \dots, Q\}$. η_{\min} is sufficiently large.

```

1: for  $j = 2 : Q$ 
2:   for  $i = 1 : j - 1$ 
3:     Calculate  $\eta_{i,j}$  using (49)
4:     if  $\eta_{\min} \geq \eta_{i,j}$ 
5:       Update  $\eta_{\min}$  by  $\eta_{i,j}$ 
6:     end
7:   end
8: end
9: Select antenna  $i, j$  according to  $\eta_{\min}$ 
10: Calculate the optimal ratio  $\lambda_{\text{opt}} = \bar{z}_i(n) / \bar{z}_j(n)$ 
Return  $\lambda_{\text{opt}}$ 

```

Subsequently, our antenna selection scheme can be described as follows. First, we compute the value of η according to (18) and (23) among $Q(Q-1)/2$ ratios. Next, we select the ratio λ_{opt} which has the minimum value of η . The detailed optimal ratio selection scheme is shown in Algorithm 2.

VI. SIMULATION RESULTS

In the simulation results presented, we assume that all the small-scale channel fading coefficients $h_q^{\text{SR}}, h_q^{\text{TR}}$ and h^{ST} follow a $\mathcal{CN}(0, 1)$ distribution. The hardware implementation loss by the Tag, α , is set as 1.1 dB [11] and the relative SNR $\Delta\gamma = 40$ dB [31]. The Monte Carlo method is used to find the BER.

A. Comparison with the Original Ratio Detector

We first compare the detection performance of the original ratio detector [29] and our proposed ratio detector. The simulated BERs versus direct link SNR of the two detectors are shown in Fig. 3. From Fig. 3, three observations can be made.

First, for the proposed ratio detector, it can be observed that the optimal ML detector (9) based on (5) and the minimum distance detector (25) based on the linearized channel (22) have almost the same BERs. This shows that the proposed linearized channel model (22) well approximates the channel (5). In addition, the BER performance of the proposed ratio detector matches well with the theoretical analysis result (34), which validates the correctness of our BER analysis.

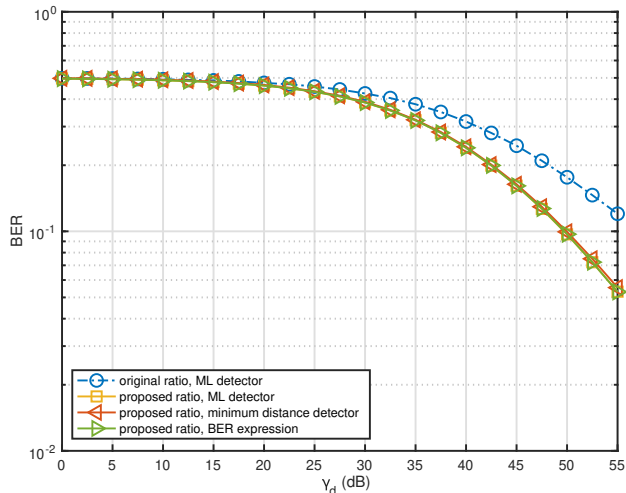


Fig. 3. BER versus the direct link SNR of the original and proposed ratio detectors.

Second, comparing the BERs of the original ratio detector and our proposed detector, we can find that at the same SNR point, the proposed ratio detector has a lower BER. This is because preserving phase information gives the detector more information.

Third, it can be seen in Fig. 3 that for both detectors, the BER curves decrease significantly when the SNR is higher than 25 dB. This is because when the data rate for the ratio detector is as high as the rate of the ambient signals, at each Tag (or ambient) symbol period, the average power of the backscattered signal is low, which results in a low receive SNR. Only when the direct link SNR is high enough, it can be ensured that the receive SNR is as high as the level that can detect the bit error. This can be overcome by averaging or coding.

It is worth noted that for our proposed ratio detector which leverages the linear channel model, the ML detector is simplified to be the minimum distance detector, which greatly reduces the detection complexity. This also allows a closed-form BER expression to be obtained. Furthermore, benefiting from the channel linearization, averaging and coding schemes can be utilized to further enhance the system performance, as will be shown in the next subsection.

B. Evaluation of Averaging and Coding

Herein we evaluate the BER performance of the averaging and coding scheme proposed in Section IV based on the accurate approximate linear channel model (22).

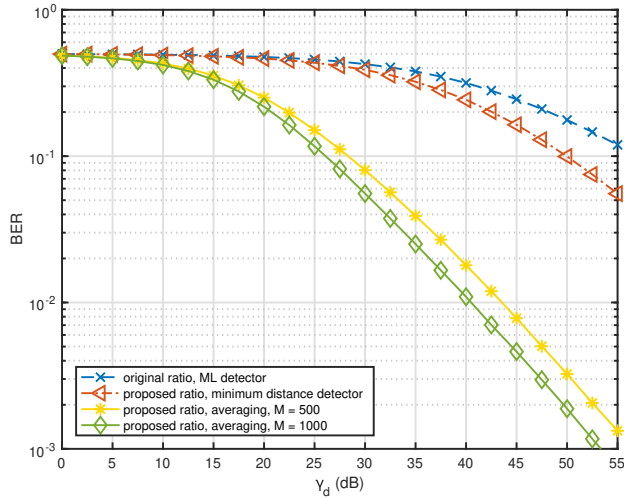


Fig. 4. BER versus the direct link SNR of the original and proposed ratio detectors with (for $M = 500$ and 1000) and without averaging.

In Fig. 4, the averaging method proposed in Section IV.A is evaluated for the proposed ratio detector, where the symbol duration is M times longer than the ambient signal period. The performance of the original ratio ML detector as well as the proposed ratio detector using minimum distance detection with no averaging is also shown as a reference. It can be seen that after averaging, the detection performance has been greatly improved. Comparing the curves of $M = 500$ and $M = 1000$, it can be seen that doubling the codeword length left shifts the BER approximately by 3 dB. However, the BER is still not ideal at the low SNR region. This is because deep fading may cause all the received samples to be lost during the bad channel condition.

In Fig. 5, hard and soft decoding with and without interleaving results are provided. The BER performance of averaging is also shown as a reference. The length of averaging duration or length of the repetition code is $M = 500$ for all the methods. In Fig. 5, three observations can be made.

First, it can be seen that although both repetition code and averaging have the same operation at the Tag side, which is to expand the duration of data (or repetition), repetition code has lower BER than averaging. This indicates that both the hard and soft decision methods have better detection performance compared with averaging the samples out.

Second, since the soft decision method considers the joint PDF of the received code word, it

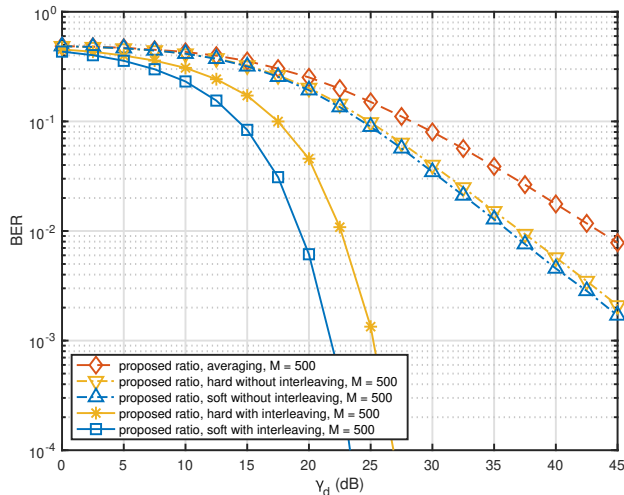


Fig. 5. BER versus the direct link SNR of the proposed ratio detector with and without interleaving when the averaging period (or length of repetition code) $M = 500$.

can be observed that it outperforms the hard decision decoding. Nevertheless, although the BER of repetition code is lower than averaging, deep fading still has considerable negative effect on detection so that the performance of using repetition code only is still not desirable.

Third, after combining the repetition code with interleaving, it can be observed that the performance improvement is impressive. The BER curves of both the soft decision method and the hard decision method drop sharply and can achieve BER at 10^{-4} level around 24 dB and 26 dB, respectively, which shows the efficiency of the encoding and detection method proposed in Section IV.C.

C. Comparison with Averaging-based Energy Detector

Fig. 6 compares the performance of our proposed ratio detector and that of the averaging-based energy detection from our previous work [31]. For our proposed ratio detector, we use the repetition code to enhance its performance and adopt soft decision method to detect the data. The scenarios with and without interleaving are both considered. The averaging period (or length of repetition code) $M = 100, 500, 1000, 2000$. From Fig. 6 we have the following observations.

First, for both kinds of detectors, the BERs decrease with increase in M when the direct link SNR is fixed. However, the ratio detector is more responsive to change in M . When M is fixed, the BER for averaging-based energy detection will not decrease when the direct link SNR is large, in other words, there is an error floor. But for the proposed ratio detector, the error

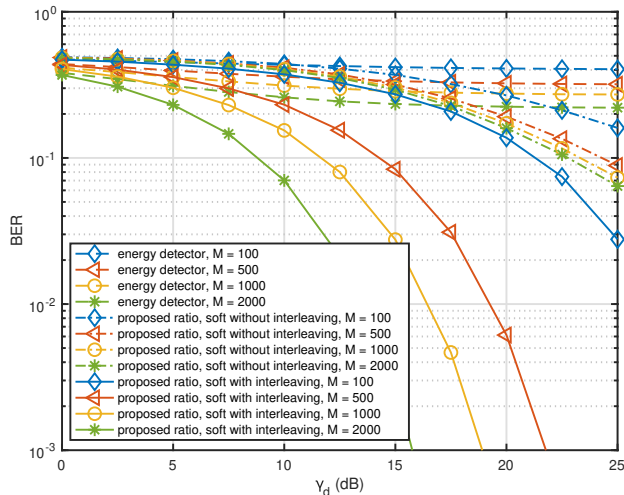


Fig. 6. BER versus direct link SNR of averaging-based energy detector and the proposed ratio detector in Section IV; averaging period (or length of repetition code) $M = 100, 500, 1000, 2000$.

floor disappears; on the contrary, the slope of the BER curve increases as the direct link SNR increases.

Second, comparing the performance of the averaging-based energy detector and ratio detector having the same M , we can find that without interleaving, and with sufficient SNR (> 20 dB), the proposed ratio detector achieves a lower BER than the averaging-based energy detector. However, after interleaving, our proposed detector always outperforms the averaging-based energy detector and the performance gap is impressive. It can be seen that when $\gamma_d = 15$ dB and $M = 1000$, the BER of the proposed detector is almost 100 times lower than energy detectors. Besides, the performance gap increases with increasing direct link SNR, which shows the superiority of our proposed ratio detector and scheme developed in Section IV.C.

One of the most important advantages of the ratio detector is the increased data rate. Therefore, in Fig. 7, we compare the BER versus M of the averaging-based energy detector and our proposed detector with repetition code. For our proposed ratio detector, hard decision decoding with interleaving have been adopted. For both of the detectors, the single-antenna Tag and dual-antenna Reader is utilized. We take three different direct link SNRs: 10, 15, 20 dB, and the following two observations can be made from Fig. 7.

First, when M is fixed, both of the detectors achieve lower BER when SNR is increased. However, the proposed ratio detector is more responsive to the change in direct link SNR. It

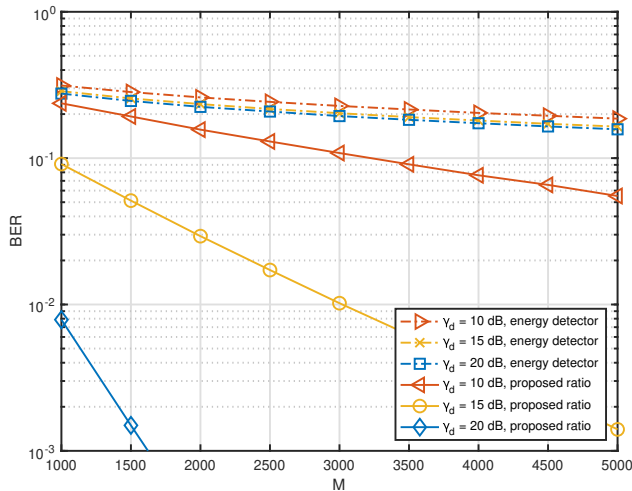


Fig. 7. BER versus M of averaging-based energy detector and our proposed ratio detector with repetition code; direct link SNR = 10, 15, 20 dB.

can be observed that for the ratio detector, the performance gap between each curve having a different SNR is much larger than that of averaging-based energy detection.

Second, for both the detectors, increasing M can improve system performance when the direct link SNR is fixed. Nevertheless, with the same direct link SNR, the proposed ratio detector has a much lower BER compared with the averaging-based energy detector and the performance gap becomes larger with increases in M .

D. Ratio Selection Scheme and Phase Compensation

To provide quantification of the gains that can be achieved with more than two antennas at the Reader, the BER performance of a 4-antenna ($Q = 4$) Reader utilizing ratio selection is shown in Fig. 8. The BER curve of a $Q = 2$ antenna system is shown as a reference. Both use interleaving to combat deep-fading and use the soft decision method to detect the Tag data. From Fig. 8 it can be seen that by implementing multiple antennas on the Reader, the ratio that has minimum η can be selected and the BER is greatly lowered compared with BER of the $Q = 2$ Reader. For $M = 500$ and $M = 1000$ cases, it can be observed that the $Q = 4$ Reader using ratio selection scheme has better performance than $Q = 2$ Reader's $M = 1000$ and $M = 2000$ cases, correspondingly. This validates the effectiveness of our proposed ratio selection scheme.

Finally, for completeness, we also investigate the effectiveness of phase compensation and the results are shown in Fig. 9. In the results, both hard and soft decision decoding with interleaving

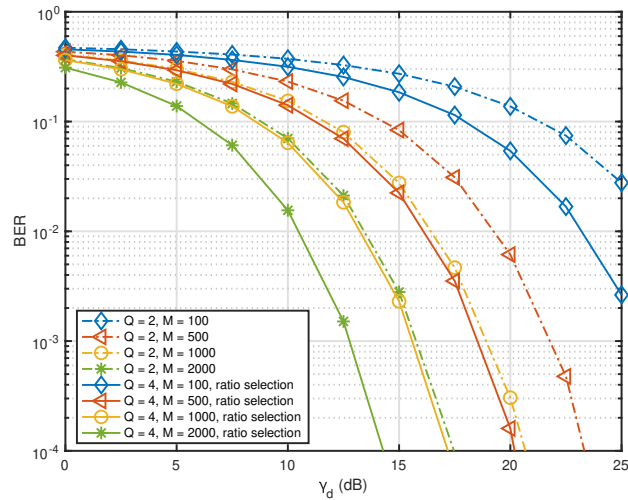


Fig. 8. BER versus direct link SNR of four-antenna Reader based on optimum ratio selection scheme; $M = 100, 500, 1000, 2000$.

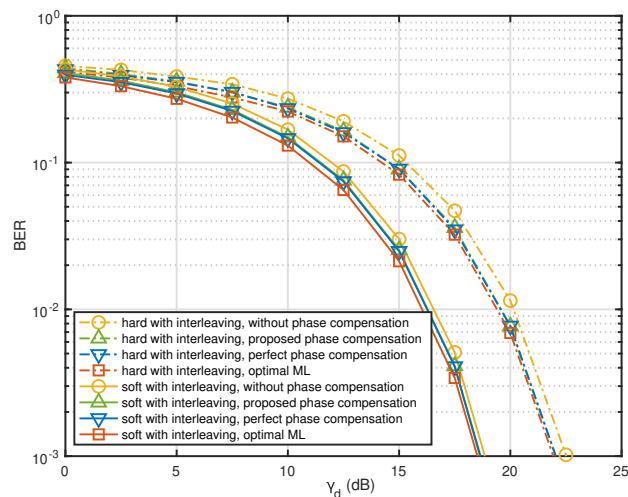


Fig. 9. Effect of phase compensation. BERs versus direct link SNR of our proposed detector with repetition code under different cases, $M = 1000$.

have been adopted and the repetition codeword length is $M = 1000$. As discussed, the left-hand side of (17) is not always equal to its right-hand side because a 2π phase shift may occur. In order to get the accurate linear channel model, it is essential to rectify the phase shift. In Fig. 9, we detect the Tag data under three different cases and compare them with the performance of optimal ML detector (9).

It can be seen that for both soft and hard decision cases, the BER performance is worst if

we detect the Tag data without any phase compensation. This is because a 2π phase shift may occur and degrade performance. After implementing the phase compensation scheme proposed in (21), we can obtain almost the same performance as perfect phase compensation, which implies that the accuracy of the proposed phase compensation is very high. Comparing the BER curves of our proposed phase compensation scheme and perfect phase compensation with the optimal performance, it can be seen that there is a small gap, which results from the approximation error of linearization. In addition, it can be seen that for both soft and hard decision cases, this performance gap decreases with the increase of SNR, since higher SNR provides a more accurate channel linearization.

Overall, the proposed phase compensation scheme can effectively solve the phase issue caused by taking the principal value of the logarithm and thus enhance the detection performance of the proposed ratio detector.

VII. CONCLUSION

In this paper, we have proposed an AmBC system with an efficient ratio detector to overcome the drawbacks of conventional averaging-based energy detectors. Unlike original ratio detectors that use the magnitude ratio of the signals between two Reader antennas, we have utilized the complex ratio so that phase information can be preserved. This allows us to devise an accurate linear model for the ratio detector, which can be utilized to open up the use of more standard detection techniques in AmBC systems. Based on the constructed linear channel model, we have proposed the minimum distance detector and derived closed-form expressions for the BER. Averaging, coding, and interleaving can also be straightforwardly applied. Besides, the results are general, allowing any number of Reader antennas to be utilized in the approach. Simulation results demonstrate that the proposed detector is better than averaging-based energy detectors and original ratio detectors. These results indicate that the proposed technique is potentially useful for future AmBC systems.

REFERENCES

- [1] A. Al-Fuqaha, M. Guizani, M. Mohammadi, M. Aledhari, and M. Ayyash, "Internet of things: A survey on enabling technologies, protocols, and applications," *IEEE Communications Surveys Tutorials*, vol. 17, no. 4, pp. 2347–2376, 2015.
- [2] F. Rezaei, C. Tellambura, and S. Herath, "Large-scale wireless-powered networks with backscatter communications—A comprehensive survey," *IEEE Open Journal of the Communications Society*, vol. 1, pp. 1100–1130, 2020.

- [3] V. Liu, A. Parks, V. Talla, S. Gollakota, D. Wetherall, and J. R. Smith, "Ambient backscatter: Wireless communication out of thin air," *ACM SIGCOMM Computer Communication Review*, vol. 43, no. 4, pp. 39–50, 2013.
- [4] S. Shen, C. Y. Chiu, and R. D. Murch, "Multiport pixel rectenna for ambient RF energy harvesting," *IEEE Trans. Antennas Propag.*, vol. 66, no. 2, pp. 644–656, Feb. 2018.
- [5] S. Shen, Y. Zhang, C.-Y. Chiu, and R. Murch, "Directional multiport ambient rf energy-harvesting system for the internet of things," *IEEE Internet Things J.*, vol. 8, no. 7, pp. 5850–5865, 2021.
- [6] N. Van Huynh, D. T. Hoang, X. Lu, D. Niyato, P. Wang, and D. I. Kim, "Ambient backscatter communications: A contemporary survey," *IEEE Communications Surveys Tutorials*, vol. 20, no. 4, pp. 2889–2922, 2018.
- [7] A. Wang, V. Iyer, V. Talla, J. R. Smith, and S. Gollakota, "FM backscatter: Enabling connected cities and smart fabrics," in *14th USENIX Symposium on Networked Systems Design and Implementation (NSDI 17)*. Boston, MA: USENIX Association, Mar. 2017, pp. 243–258. [Online]. Available: <https://www.usenix.org/conference/nsdi17/technical-sessions/presentation/wang-anran>
- [8] S. N. Daskalakis, J. Kimionis, A. Collado, G. Goussetis, M. M. Tentzeris, and A. Georgiadis, "Ambient backscatterers using FM broadcasting for low cost and low power wireless applications," *IEEE Trans. Microw. Theory Techn.*, vol. 65, no. 12, pp. 5251–5262, 2017.
- [9] B. Kellogg, A. Parks, S. Gollakota, J. R. Smith, and D. Wetherall, "Wi-Fi backscatter: Internet connectivity for RF-powered devices," in *Proceedings of the 2014 ACM Conference on SIGCOMM*, 2014, pp. 607–618.
- [10] D. Bharadia, K. R. Joshi, M. Kotaru, and S. Katti, "Backfi: High throughput WiFi backscatter," *ACM SIGCOMM Computer Communication Review*, vol. 45, no. 4, pp. 283–296, 2015.
- [11] B. Kellogg, V. Talla, S. Gollakota, and J. R. Smith, "Passive Wi-Fi: Bringing low power to Wi-Fi transmissions," in *13th USENIX Symposium on Networked Systems Design and Implementation (NSDI 16)*. Santa Clara, CA: USENIX Association, Mar. 2016, pp. 151–164. [Online]. Available: <https://www.usenix.org/conference/nsdi16/technical-sessions/presentation/kellogg>
- [12] B. Ji, B. Xing, K. Song, C. Li, H. Wen, and L. Yang, "The efficient BackFi transmission design in ambient backscatter communication systems for IoT," *IEEE Access*, vol. 7, pp. 31 397–31 408, 2019.
- [13] Q. Zhang, H. Guo, Y. Liang, and X. Yuan, "Constellation learning-based signal detection for ambient backscatter communication systems," *IEEE J. Sel. Areas Commun.*, vol. 37, no. 2, pp. 452–463, 2019.
- [14] G. Wang, F. Gao, R. Fan, and C. Tellambura, "Ambient backscatter communication systems: Detection and performance analysis," *IEEE Trans. Commun.*, vol. 64, no. 11, pp. 4836–4846, 2016.
- [15] G. Wang, F. Gao, Z. Dou, and C. Tellambura, "Uplink detection and ber analysis for ambient backscatter communication systems," in *2015 IEEE Global Communications Conference (GLOBECOM)*, 2015, pp. 1–6.
- [16] J. Qian, F. Gao, G. Wang, S. Jin, and H. Zhu, "Semi-coherent detection and performance analysis for ambient backscatter system," *IEEE Trans. Commun.*, vol. 65, no. 12, pp. 5266–5279, 2017.
- [17] —, "Noncoherent detections for ambient backscatter system," *IEEE Trans. Wireless Commun.*, vol. 16, no. 3, pp. 1412–1422, 2017.
- [18] J. Qian, A. N. Parks, J. R. Smith, F. Gao, and S. Jin, "IoT communications with M -PSK modulated ambient backscatter: Algorithm, analysis, and implementation," *IEEE Internet Things J.*, vol. 6, no. 1, pp. 844–855, 2019.
- [19] Q. Tao, C. Zhong, H. Lin, and Z. Zhang, "Symbol detection of ambient backscatter systems with Manchester coding," *IEEE Trans. Wireless Commun.*, vol. 17, no. 6, pp. 4028–4038, 2018.
- [20] S. Guruacharya, X. Lu, and E. Hossain, "Optimal non-coherent detector for ambient backscatter communication system," *IEEE Trans. Veh. Technol.*, vol. 69, no. 12, pp. 16 197–16 201, 2020.

- [21] Q. Tao, C. Zhong, X. Chen, H. Lin, and Z. Zhang, "Optimal detection for ambient backscatter communication systems with multi-antenna reader under complex gaussian illuminator," *IEEE Internet Things J.*, vol. 7, no. 12, pp. 11 371–11 383, 2020.
- [22] H. Guo, Q. Zhang, S. Xiao, and Y. Liang, "Exploiting multiple antennas for cognitive ambient backscatter communication," *IEEE Internet Things J.*, vol. 6, no. 1, pp. 765–775, 2019.
- [23] Z. Ma, T. Zeng, G. Wang, and F. Gao, "Signal detection for ambient backscatter system with multiple receiving antennas," in *2015 IEEE 14th Canadian Workshop on Information Theory (CWIT)*, 2015, pp. 50–53.
- [24] M. A. ElMossallamy, M. Pan, R. Jäntti, K. G. Seddik, G. Y. Li, and Z. Han, "Noncoherent backscatter communications over ambient OFDM signals," *IEEE Trans. Commun.*, vol. 67, no. 5, pp. 3597–3611, 2019.
- [25] Q. Tao, C. Zhong, K. Huang, X. Chen, and Z. Zhang, "Ambient backscatter communication systems with MFSK modulation," *IEEE Trans. Wireless Commun.*, vol. 18, no. 5, pp. 2553–2564, 2019.
- [26] G. Vougioukas and A. Bletsas, "Switching frequency techniques for universal ambient backscatter networking," *IEEE J. Sel. Areas Commun.*, vol. 37, no. 2, pp. 464–477, 2019.
- [27] T. Zeng, G. Wang, Y. Wang, Z. Zhong, and C. Tellambura, "Statistical covariance based signal detection for ambient backscatter communication systems," in *2016 IEEE 84th Vehicular Technology Conference (VTC-Fall)*, 2016, pp. 1–5.
- [28] A. N. Parks, A. Liu, S. Gollakota, and J. R. Smith, "Turbocharging ambient backscatter communication," *ACM SIGCOMM Computer Communication Review*, vol. 44, no. 4, pp. 619–630, 2014.
- [29] S. Ma, G. Wang, Y. Wang, and Z. Zhao, "Signal ratio detection and approximate performance analysis for ambient backscatter communication systems with multiple receiving antennas," *Mobile Networks and Applications*, vol. 23, no. 6, pp. 1478–1486, 2018.
- [30] X. Wang, H. Yiğitler, R. Duan, E. Y. Menta, and R. Jäntti, "Coherent multi-antenna receiver for BPSK-modulated ambient backscatter tags," *IEEE Internet Things J.*, vol. 9, no. 2, pp. 1197–1211, 2022.
- [31] W. Liu, S. Shen, D. H. K. Tsang, and R. Murch, "Enhancing ambient backscatter communication utilizing coherent and non-coherent space-time codes," *IEEE Trans. Wireless Commun.*, vol. 20, no. 10, pp. 6884–6897, 2021.
- [32] R. J. Baxley, B. T. Walkenhorst, and G. Acosta-Marum, "Complex gaussian ratio distribution with applications for error rate calculation in fading channels with imperfect CSI," in *2010 IEEE Global Telecommunications Conference GLOBECOM 2010*, 2010, pp. 1–5.
- [33] W.-J. Yan and W.-X. Ren, "Generalized proper complex gaussian ratio distribution and its application to statistical inference for frequency response functions," *J. Eng. Mech.*, vol. 144, no. 9, p. 04018080, 2018.
- [34] S. Ma, G. Wang, R. Fan, and C. Tellambura, "Blind channel estimation for ambient backscatter communication systems," *IEEE Commun. Lett.*, vol. 22, no. 6, pp. 1296–1299, 2018.
- [35] S. Ma, Y. Zhu, G. Wang, and R. He, "Machine learning aided channel estimation for ambient backscatter communication systems," in *2018 IEEE International Conference on Communication Systems (ICCS)*, 2018, pp. 67–71.
- [36] T. Y. Kim and D. I. Kim, "Novel sparse-coded ambient backscatter communication for massive IoT connectivity," *Energies*, vol. 11, no. 1780, pp. 1–25, Jul. 2018.
- [37] W. Zhao, G. Wang, S. Atapattu, R. He, and Y. Liang, "Channel estimation for ambient backscatter communication systems with massive-antenna reader," *IEEE Trans. Veh. Technol.*, vol. 68, no. 8, pp. 8254–8258, 2019.
- [38] D. Darsena, G. Gelli, and F. Verde, "Joint channel estimation, interference cancellation, and data detection for ambient backscatter communications," in *2018 IEEE 19th International Workshop on Signal Processing Advances in Wireless Communications (SPAWC)*, 2018, pp. 1–5.
- [39] X. Liu, C. Liu, Y. Li, B. Vucetic, and D. W. K. Ng, "Deep residual learning-assisted channel estimation in ambient backscatter communications," *IEEE Wireless Commun. Lett.*, vol. 10, no. 2, pp. 339–343, 2021.